



Mercury distribution and transport in the North Atlantic Ocean along the GEOTRACES-GA01 transect

Daniel Cossa¹, Lars-Eric Heimbürger², Fiz F. Pérez³, Maribel I. García-Ibáñez^{4,3}, Jeroen E. Sonke⁵, Hélène Planquette⁶, Pascale Lherminier⁷, Julia Boutorh⁶, Marie Cheize⁶, Jan Lukas Menzel Barraqueta⁸, Rachel Shelley⁶, and Géraldine Sarthou⁶

¹ISTerre, Université Grenoble Alpes, CS 40700, 38058 Grenoble Cedex 9, France

²Aix Marseille Université, CNRS/INSU, Université de Toulon, IRD, Mediterranean Institute of Oceanography (MIO) UM 110, Marseille, France

³Instituto de Investigaciones Marinas, CSIC, Eduardo Cabello 6, 36208 Vigo, Spain

⁴Uni Research Climate, Bjerknes Centre for Climate Research, Bergen 5008, Norway

⁵CNRS, GET-OMP, 14 Ave. E. Belin, 31240 Toulouse, France

⁶LEMAR, Université de Bretagne Occidentale, 29280 Plouzané, France

⁷IFREMER, Brittany Center, LPO, BP 70, 29280 Plouzané, France

⁸GEOMAR, Helmholtz Centre for Ocean Research, 24148 Kiel, Germany

Correspondence: Daniel Cossa (dcossa@ifremer.fr)

Received: 31 October 2017 – Discussion started: 13 November 2017

Revised: 23 February 2018 – Accepted: 3 March 2018 – Published: 19 April 2018

Abstract. We report here the results of total mercury (HgT) determinations along the 2014 GEOTRACES GEOVIDE cruise (GA01 transect) in the North Atlantic Ocean (NA) from Lisbon (Portugal) to the coast of Labrador (Canada). HgT concentrations in unfiltered samples (HgT_{UNF}) were log-normally distributed and ranged between 0.16 and 1.54 pmol L⁻¹, with a geometric mean of 0.51 pmol L⁻¹ for the 535 samples analysed. The dissolved fraction (< 0.45 μm) of HgT (HgT_F), determined on 141 samples, averaged 78 % of the HgT_{UNF} for the entire data set, 84 % for open seawaters (below 100 m) and 91 % if the Labrador Sea data are excluded, where the primary production was high (with a winter convection down to 1400 m). HgT_{UNF} concentrations increased eastwards and with depth from Greenland to Europe and from subsurface to bottom waters. The HgT_{UNF} concentrations were similarly low in the subpolar gyre waters (~ 0.45 pmol L⁻¹), whereas they exceeded 0.60 pmol L⁻¹ in the subtropical gyre waters. The HgT_{UNF} distribution mirrored that of dissolved oxygen concentration, with highest concentration levels associated with oxygen-depleted zones. The relationship between HgT_F and the apparent oxygen utilization confirms the nutrient-like behaviour of Hg in the NA. An extended optimum multiparameter analysis allowed us to

characterize HgT_{UNF} concentrations in the different source water types (SWTs) present along the transect. The distribution pattern of HgT_{UNF}, modelled by the mixing of SWTs, show Hg enrichment in Mediterranean waters and North East Atlantic Deep Water and low concentrations in young waters formed in the subpolar gyre and Nordic seas. The change in anthropogenic Hg concentrations in the Labrador Sea Water during its eastward journey suggests a continuous decrease in Hg content in this water mass over the last decades. Calculation of the water transport driven by the Atlantic Meridional Overturning Circulation across the Portugal–Greenland transect indicates northward Hg transport within the upper limb and southward Hg transport within the lower limb, with resulting net northward transport of about 97.2 kmol yr⁻¹.

1 Introduction

The ocean plays a central role in the global mercury (Hg) cycle. It receives Hg mainly from atmospheric deposition, whereas it disposes of it in deep marine sediments (e.g. Mason et al., 1994). In the meantime, the largest part of Hg is recycled in the atmosphere, while a smaller fraction pene-

trates the ocean interior via thermohaline circulation or the biological pump (see reviews by Mason and Sheu, 2002; Fitzgerald et al., 2007; Mason et al., 2012). Firstly, Hg re-injection to the atmosphere results from the formation of volatile elemental Hg via photoreduction and microbiological reduction of divalent Hg (e.g. Mason et al., 1995; Amyot et al., 1997). Secondly, Hg integration into the thermohaline circulation involves its solubilization in surface waters followed by the subduction of these water masses along isopycnals (e.g. Gill and Fitzgerald, 1988). Thirdly, the biological pump consists of Hg sorption onto biogenic particles produced in the euphotic zone. Then it conveys sinking materials at depth with possible Hg remobilization due to the particulate remineralization–dissolution process (e.g. Mason and Fitzgerald, 1993). The shape of observed vertical oceanic Hg profiles, characterized by increasing concentrations with depth, includes the marks of these different routes and is akin to nutrient-type profiles (Gill and Fitzgerald, 1988; Cossa et al., 2004; Lamborg et al., 2014; Bowman et al., 2015, 2016). The Hg cycle is also known for being highly perturbed by human activities (e.g. Mason et al., 2012; Lamborg et al., 2014; Zhang et al., 2014; Amos et al., 2015). Modern Hg concentrations in the global atmosphere are more than 3 times the pre-industrial Hg concentrations, leading to increasing Hg concentrations in surface and intermediate oceanic layers, which remain to be precisely estimated. Despite these advances in knowledge of the Hg biogeochemical cycle, the key features of the Hg distribution among the principal oceanic water masses are still poorly documented. Recent enhancements in the precision of Hg analyses allow more reliable vertical Hg profiles in the water columns (e.g. Cossa et al., 2011; Lamborg et al., 2014; Heimbürger et al., 2015; Bowman et al., 2015, 2016; Munson et al., 2015; Cossa et al., 2017a, b). In addition, an original approach for the estimation of the anthropogenic fractions of Hg concentrations in oceanic waters has been proposed (Lamborg et al., 2014). Owing to these last methodological breakthroughs, significant advances in detailed Hg oceanic distributions are possible.

The North Atlantic Ocean (NA) plays an active role in the cycling of chemical species in the ocean because it is a region where deep water formation drives the Atlantic Meridional Overturning Circulation (AMOC) (Kuhlbrodt et al., 2007). Particularly in the subpolar NA, chemical properties, including Hg, are transported to the ocean interior; thus, NA offers a unique opportunity for studying the oceanic response to changes in atmospheric Hg deposition. The GEOTRACES-GA03 zonal and meridional transects, sampled in 2010 and 2011, covered the NA from east to west between 18 and 40° N, from the coast of Africa to the coast of the USA. Here, we report the results of the GEOVIDE cruise along the GEOTRACES-GA01 transect, which targeted the NA from 40 to 60° N, from Portugal to Newfoundland via the southern tip of Greenland (Fig. 1). This article provides (i) a high-resolution description of the HgT distribution in the waters

of the subpolar and subtropical gyres of the NA, (ii) characterization the HgT concentrations of the main water masses of the NA, (iii) an estimate of the temporal change of anthropogenic Hg in LSW and (iv) quantification of the HgT transport associated with the upper and lower limbs of the AMOC. These new data contribute to a refinement of the depiction of the Hg distribution in the NA waters and should allow further improvements in the oceanic Hg modelling.

2 Oceanographic context

A full description of the water masses along the GEOTRACES-GA01 transect can be found in García-Ibáñez et al. (2018). Briefly, the North Atlantic Current (NAC) conveys the warm salty surface waters from subtropical regions northwards to the subpolar regions, where they are cooled down by heat exchange with the atmosphere (Fig. 1). The intermediate and deep waters formed this way fill up the Global Ocean, initiating the southward-flowing limb of the AMOC (e.g. McCartney and Talley, 1984; Lherminier et al., 2010). In addition, the general circulation pattern is characterized by the subtropical and the subpolar gyres (Fig. 1).

In the subtropical gyre (Fig. 1), several water masses can be identified. They are listed from top to bottom: (i) the mixed layer, (ii) the eastern North Atlantic Central Water (ENACW), (iii) the Mediterranean waters (MW), (iv) the Labrador Sea Water (LSW) and (v) the Lower North East Atlantic Deep Water (NEADW_L), which contains about 30 % Antarctic Bottom Water (AABW) (García-Ibáñez et al., 2015). The transformation of ENACW leads to the formation of different mode waters including the Subpolar Mode Waters (SPMWs) (McCartney and Talley, 1982; Tsuchiya et al., 1992; van Aken and Becker, 1996; Brambilla and Talley, 2008; Cianca et al., 2009). SPMWs are the near-surface water masses of the subpolar gyre of the NA characterized by thick layers of nearly uniform temperature, often denoted with temperature in subscript (SPMW₈, for example). SPMWs are formed during winter convection at high latitudes due to atmospheric freshening of surface waters originating from the subtropical gyre (McCartney, 1992). SPMWs participate in the upper limb of the AMOC and provide much of the water that is eventually transformed into the several components of North Atlantic Deep Water (NADW; Brambilla and Talley, 2008).

In the subpolar gyre, ocean–atmosphere interaction is particularly intense. The cooling down of subtropical waters produces dense waters, triggering the deepening of the mixed layer and further leading to deep convection. The main NA convection zones are located in the Labrador (LS), Irminger (IrS) and Nordic seas (NS) (Fig. 1). Convection in those zones leads to the formation of intermediate and deep waters such as LSW, Denmark Strait Overflow Water (DSOW) and Iceland–Scotland Overflow Water (ISOW). LSW and ISOW are the main components of NEADW, and the all three are

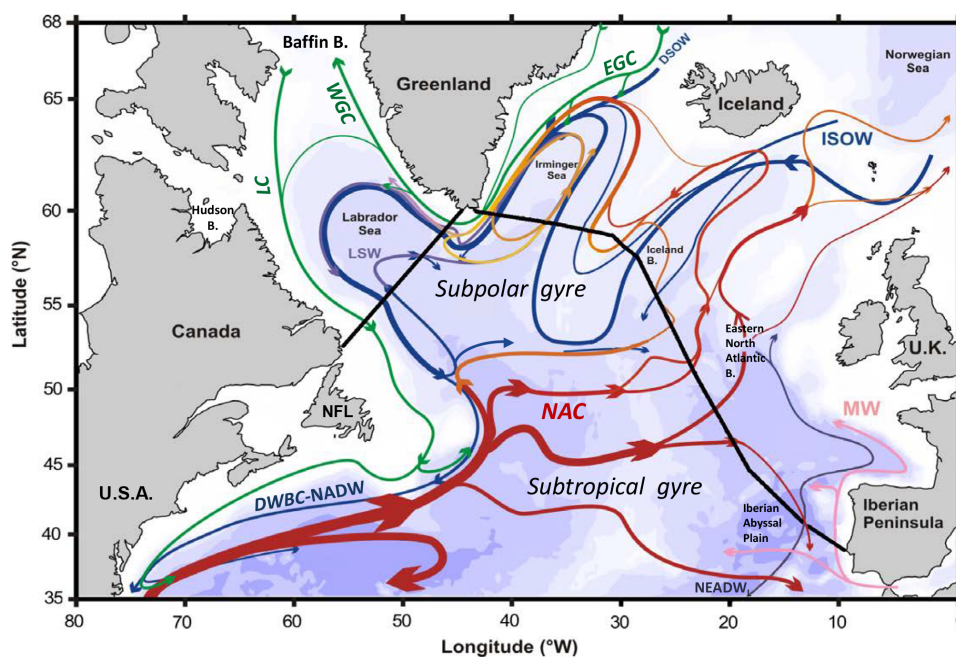


Figure 1. Schematic view of the water circulation in the North Atlantic Ocean adapted from García-Ibáñez et al. (2015) and Danialt et al. (2016). Red lines indicate the circulation in surface, while blue lines indicated circulation at depth. Black lines represent the GEOVIDE cruise that transects (GEOTRACES-GA01). The main geographical features, water masses and currents are indicated: Newfoundland (NFL), United Kingdom (UK), United States of America (USA), Denmark Strait Overflow Water (DSOW), Iceland–Scotland Overflow water (ISOW), Labrador Sea Water (LSW), Lower North East Atlantic Deep Water (NEADW_L), Mediterranean waters (MW) and North Atlantic Deep Water (NADW), Deep Western Boundary Current (DWBC), East Greenland Current (EGC), Labrador Current (LC), North Atlantic Current (NAC) and West Greenland Current (WGC).

components of the NADW, which constitutes the cold deep limb of the AMOC, flowing southward towards the Southern Ocean in the western Atlantic basin. LSW has been variably produced in the past 50 years, depending on the intensity of winter convection, linked to the intensity of the North Atlantic Oscillation (e.g. Rhein et al., 2002; Cianca et al., 2009; Yashayaev and Loder, 2016). Depths of winter convection in the LS vary from a few hundred metres (the early 2000s) to over 2000 m (early 1990s). The LSW is a thick layer in the LS but thins out as it travels south-westwardly. It spreads out into the entire NA, filling the subpolar gyre and entering the subtropical gyre. Within the subpolar gyre, LSW is marked by a salinity minimum above the ISOW. In both gyres, the well-ventilated LSW has a marked oxygen maximum.

3 Materials and methods

3.1 Sampling

Water samples were collected during the French-led GEOVIDE cruise (GEOTRACES-GA01 transect), on board the RV *Pourquoi Pas?* sailing from Lisbon (Portugal) on 15 May and arriving on 30 June 2014 in St John's (Newfoundland, Canada) (Fig. 1). Seventy-eight (78) stations (Table S1 in

the Supplement) were occupied for hydrographic profiles (CTD, dissolved oxygen, nutrients), of which 29 included trace-metal sampling. Sampling and water treatment for HgT determination (Lamborg et al., 2012; Cutter et al., 2017) were performed using ultra-trace techniques following the GEOTRACES recommendations. During the GEOVIDE cruise, an epoxy-coated aluminum rosette, equipped with 12 L GO-FLO (General Oceanics©) bottles initially cleaned following the GEOTRACES procedures (Cutter and Bruland, 2012), was deployed on a 6 mm Kevlar hydrowire. The rosette was also equipped with probes for pressure, conductivity, temperature, dissolved oxygen, fluorometry and transmission measurements (titanium SBE model 911-plus, Sea-Bird Electronics®). Specifically for Hg determination, all materials in contact with the seawater samples were made of Teflon or were Teflon coated, acid cleaned and rinsed with ultrapure water (Milli-Q, Millipore®) prior to utilization. Original vent fixture and sampling valves of the GO-FLO bottles were replaced with Teflon (PTFE) ones. GO-FLO bottles were subsampled under a laminar flow bench inside a clean trace-metal container. The efficiency of the high-efficiency particulate air filter (HEPA, 0.3 µm) in the container was checked with a Coulter counter during the cruise. All subsequent sample treatments (including filtration) and Hg analyses were also performed in clean class 100 containers. For sample

filtrations, acid-washed 0.45 μm polycarbonate membranes (Nuclepore) were preferred to cellulose acetate or polyether-sulfone membranes proposed in the GEOTRACES protocols (Fig. S1 in the Supplement). Subsamples were stored in Teflon bottles (FEP) until the on board HgT analyses, which occurred within 6 h after sampling.

3.2 Chemical analyses

In order to access all Hg species, the release of Hg from its ligands was achieved by a BrCl solution (50 μL of a 0.2 N solution is added to a 40 mL sample), and then the Hg was reduced with an acidic SnCl_2 solution (100 μL of a 1 M solution is added to a 40 mL sample). Potassium bromide (Sigma Aldrich, USA) and potassium bromate (Sigma Aldrich, USA) were heated for 4 h at 250 $^\circ\text{C}$ to remove Hg traces before making up BrCl solution with freshly double-distilled HCl (Heimbürger et al., 2015). The generated Hg vapour was amalgamated into a gold trap and then released by heating into an atomic fluorescence spectrometer (AFS). We used two AFS systems in parallel (Tekran[®] Model 2500, Brooks[®] Model 3), both calibrated against the NIST 3133 (National Institute of Standards and Technology) certified reference material. This technique, initially described by Bloom and Crecelius (1983) and subsequently improved by Gill and Fitzgerald (1985), is now an authoritative procedure officialised by the US EPA as method 1631 (Environmental Protection Agency, 2002). The definitions of detection limit (DL), reproducibility and accuracy given here are adopted from Taylor (1987) and Hewitt (1989). Using a mirrored quartz cuvette (Hellma[®]) allowed for an “absolute DL”, defined as 2 times the electronic noise magnitude, as low as 1.7 femtomoles. However, in practice for trace measurements, the DL is governed by the reproducibility of the blank values and calculated as 3.3 times the standard deviation of blank values. The blank values were determined on a purged Hg-free seawater sample spiked with reagents (i.e. BrCl and SnCl_2). The mean (\pm standard deviation) of blank values measured during the GEOVIDE cruise was 3.2 ± 1.0 femtomoles. Thus, for a 40 mL seawater aliquot, the DL expressed in HgT concentration was 0.07 pmol L^{-1} . The reproducibility (coefficient of variation of six replicate measures) varied according to the concentration level between 5 and 15 %. The accuracy of HgT measurements was tested using ORMS-5 certified reference material (CRM) from the National Research Council of Canada (<http://www.nrc-cnrc.gc.ca/>, last access: April 2018) and spiked to a purged Hg-free seawater sample. Measurements were always within the given confidence interval. To ensure good data quality and to continue previous efforts (Cossa and Courau, 1990; Lamborg et al., 2012), we organized the 2014 GEOTRACES intercalibration exercise for total HgT and methyl Hg as a part of the GEOVIDE cruise. The intercalibration sample was taken on 22 June 2014 in the LS at 49.093 $^\circ$ W, 55.842 $^\circ$ N, and 2365 m depth. The sample was sent out to 10 participating

laboratories. This station was also planned as crossover station within the 2015 Arctic GEOTRACES effort (Canadian cruise) but has subsequently been changed to another location. Our results compare well with the consensus values, $\text{HgT} = 0.63 \pm 0.12 \text{ pmol L}^{-1}$, $n = 8$. We measured the 2014 GEOTRACES intercalibration sample twice for HgT and obtained 0.51 (22 June 2014, on board) and 0.58 pmol L^{-1} (30 October 2014, home lab).

3.3 Extended optimum multiparameter analysis

We used an extended optimum multiparameter (eOMP) analysis to characterize the water mass HgT_{UNF} concentrations along the GEOTRACES-GA01 transect (García-Ibáñez et al., 2015, 2018). The eOMP analysis quantifies the proportions of the different source water types (SWTs) that contribute to a given water sample. The HgT_{UNF} concentration of each SWT, $[\text{HgT}_{\text{UNF}}]_i$, was estimated through an inversion of the SWT fractions given by the eOMP analysis. This approach was successfully applied to dissolved organic carbon water mass definitions in the NA (Fontela et al., 2016) and to evaluate the impact of water mass mixing and remineralization on the N_2O distribution in the NA (de la Paz et al., 2017). Here, we performed an inversion of a system of 430 equations (HgT_{UNF} samples) and 11 unknowns ($[\text{HgT}_{\text{UNF}}]_i$). Samples for which the difference between the observed HgT_{UNF} and the predicted HgT_{UNF} values by the multiple linear regression (Eq. 1 below) was 3 times greater than the standard deviation were removed from the analysis. Nine samples were used: Station 2 (125 m), Station 11 (793 m), Station 11 (5242 m), Station 13 (1186 m), Station 15 (170 m), Station 19 (99 m), Station 26 (97 m), Station 32 (596 m) and Station 38 (297 m). The SWTs were characterized by potential temperature, salinity, and macronutrients. The eOMP was restricted to depths below 75 m in order to avoid air–sea interaction effects. The eOMP gave us the fractions of the 11 SWTs, and we resolved the following expression to estimate the $[\text{HgT}_{\text{UNF}}]_i$:

$$[\text{HgT}_{\text{UNF}}]_j = \sum_{i=1}^{11} \text{SWT}_i^j \times [\text{HgT}_{\text{UNF}}]_i + \varepsilon_j \quad (j = 1 \dots 430), \quad (1)$$

where $[\text{HgT}_{\text{UNF}}]_j$ represents the measured HgT_{UNF} concentration for each sample j , SWT_i^j the proportion of SWT i to sample j (obtained through the eOMP), $[\text{HgT}_{\text{UNF}}]_i$ the HgT_{UNF} concentration for each SWT i (unknown), and ε_j the residual. The 430 ε_j s of the inversion presented a null mean and a standard deviation of $0.085 \text{ pmol L}^{-1}$ ($R = 0.84$).

3.4 Mercury transport calculation

Velocity fields across the GEOTRACES-GA01 transect were calculated using an inverse model constrained by Doppler current profiler velocity measurements (Zunino et al., 2017)

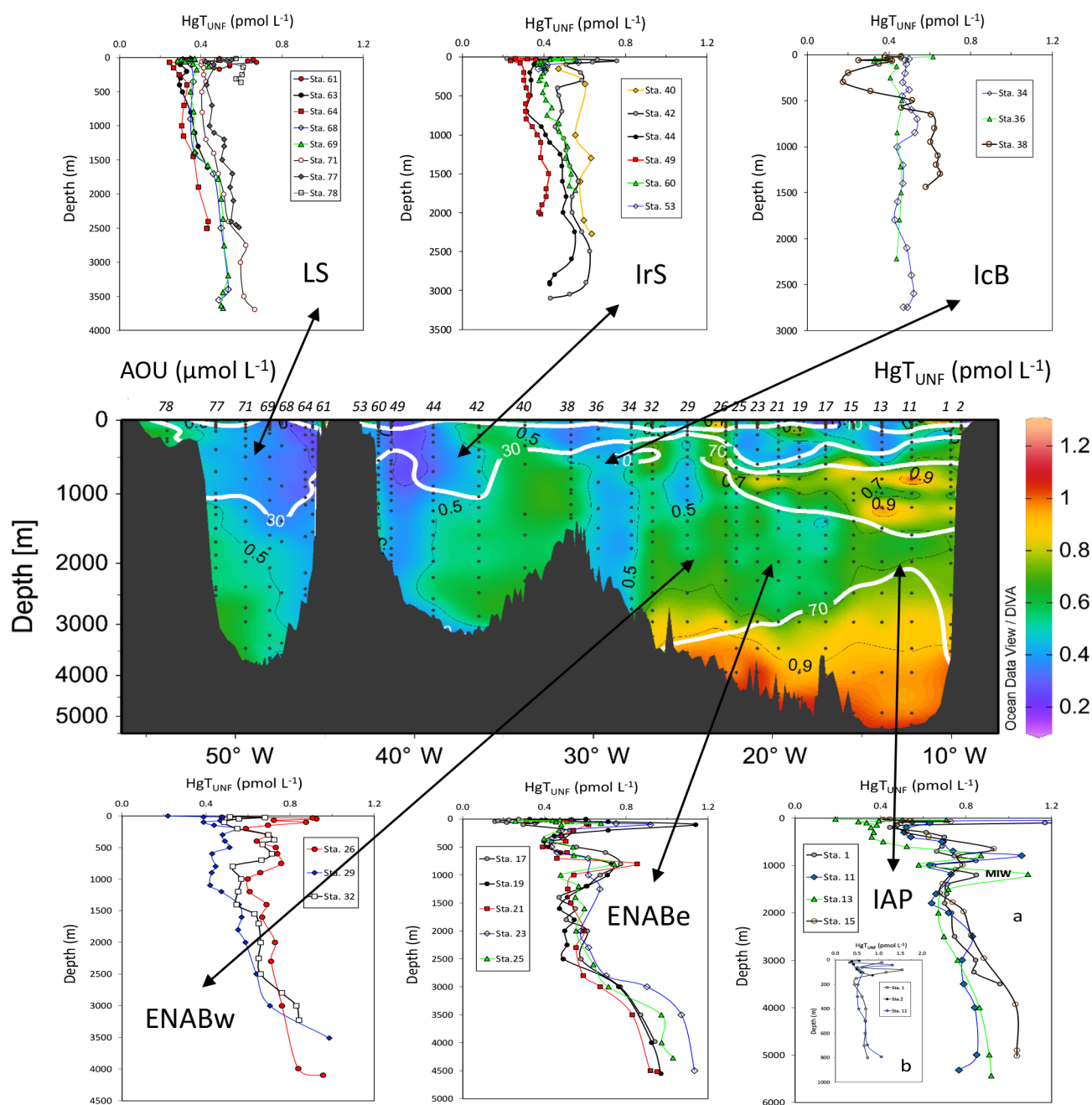


Figure 2. Distribution of unfiltered total mercury (HgT_{UNF}) concentrations along the GEOTRACES-GA01 transect. LS: Labrador Sea; IrS: Irminger Sea; IcB: Iceland basin; ENABw: western part of the eastern North Atlantic basin; ENABe: eastern part of the eastern North Atlantic basin; IAP: Iberian Abyssal Plain.

an overall mass balance of 1 ± 3 Sv to the north (Lherminier et al., 2007, 2010). The volume transport per SWT was computed by combining these velocity fields with the results of the eOMP (García-Ibáñez et al., 2018). Finally, the HgT_{UNF} transport per water mass was calculated through Eq. (2):

$$T_{HgT_{UNF}} = \sum_{i=1}^{11} T_{SWT_i} \times [HgT_{UNF}]_i \times \rho_i, \quad (2)$$

where T_{SWT_i} is the volume transport of SWT i , $[HgT_{UNF}]_i$ is the HgT_{UNF} concentration for each SWT i (from Eq. 1), and ρ_i is the density of the SWT i .

The inverse model configuration for the GEOVIDE cruise data is described in Zunino et al. (2017). The inverse model is based on the least squares formalism, which provides errors on the velocities and associated quantities such as the magnitude of the AMOC (estimated in density coordinate) and the

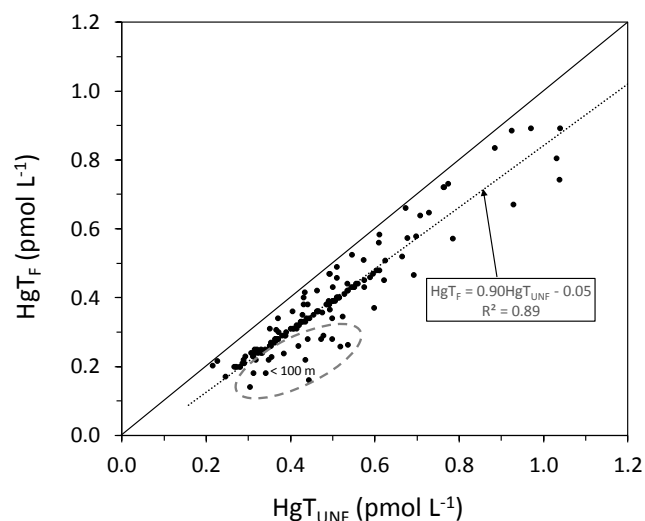


Figure 3. Mercury concentrations in filtered (HgT_F) vs. unfiltered (HgT_{UNF}) samples ($n = 141$) collected along the GEOTRACES-GA01 transect.

heat flux (Lherminier et al., 2010). The inverse model computes the absolute geostrophic transport orthogonal to the section. The Ekman transport is deduced from the wind fields averaged over the cruise period and added homogeneously to the upper 40 m (Mercier et al., 2015). The transport estimates of the inverse model across the section have been validated by favourable comparisons with independent measurements (Gourcuff et al., 2011; Danialt et al., 2011; Mercier et al., 2015).

4 Results

Distributions of potential temperature, salinity, dissolved oxygen and silicic acid are given in García-Ibáñez et al. (2018),

HgT_{UNF} concentrations along the GEOTRACES-GA01 transect ranged from 0.16 to 1.54 pmol L^{-1} ($n = 535$), these data being log-normally distributed, positively skewed (Skewness = 1.1; Kurtosis = 2.1; Fig. S3) and having 97 % of the values lower than 1.00 pmol L^{-1} . The geometric mean and the median were 0.51 pmol L^{-1} , whereas the arithmetic mean and standard deviation were 0.54 and 0.19 pmol L^{-1} , respectively. These concentrations are within the range found along the GEOTRACES-GA03 transect (0.09–1.89 pmol L^{-1} , $n = 605$) that crossed the NA within the subtropical gyre from 18 to 40° N (Bowman et al., 2015), but are lower than the range and the unusually high arithmetic mean determined in the South Atlantic along the GEOTRACES-GA10 transect (0.39–3.39 pmol L^{-1} , $n = 375$; Arne Bratkič, personal communication, 2017 and 1.45 ± 0.60 pmol L^{-1} ; Bratkič et al., 2016).

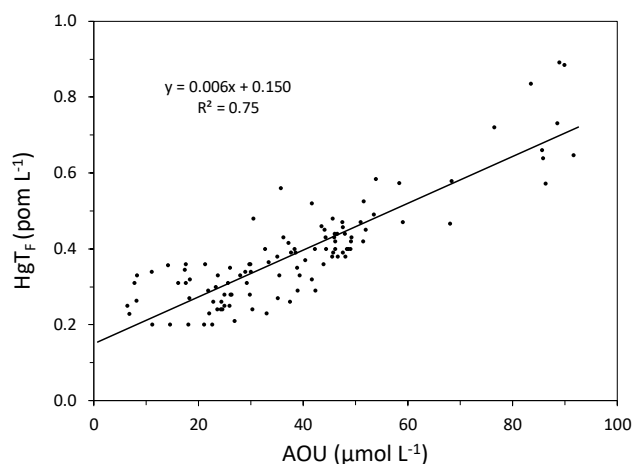


Figure 4. Total Hg in filtered samples (HgT_F) vs. apparent oxygen utilization (AOU) along the GEOTRACES-GA01 transect.

The overall distribution of the HgT_{UNF} concentrations along the GEOTRACES-GA01 transect is represented in Fig. 2. The main features of HgT_{UNF} concentrations are an eastward increase from Greenland to Europe and a downward increase from subsurface to bottom waters. In addition, the lowest and highest (most variable) HgT_{UNF} values were encountered in surface and subsurface waters, where Hg evasion to the atmosphere and high particulate matter concentrations may generate low and high HgT_{UNF} concentrations, respectively. Out of the 141 filtered samples that were analysed, altogether, the filtered fraction of Hg (HgT_F) represents, on average, 78 % (range: 36–98 %) of the HgT_{UNF} (Fig. 3). Excluding the upper 100 m, where the biogenic suspended particles are usually abundant, and the stations located on the shelf and slope, where particulate matter from continental sources are usually present, the HgT_F fraction represents, on average, 84 % (range: 72–98 %) of the HgT_{UNF} . In addition, in the LS, $\text{HgT}_F / \text{HgT}_{UNF}$ mean ratios were rather low ranging 62–92 %, with a mean of 76 %. In fact, the primary production was high in spring 2014 in LS, and the winter convection, which reached 1400 m, conveyed surface particles at depth (Yashayaev et al., 2015; Lemaitre et al., 2017). If we exclude the LS from the HgT_F mean computation, we obtain a mean percentage $\text{HgT}_F / \text{HgT}_{UNF}$ ratio of 91 %, which is similar to values (~90 %) obtained along the GEOTRACES-GA03 zonal and meridional transects (Bowman et al., 2015). In the following subsections, detailed descriptions of the HgT_{UNF} profiles for the five following oceanographic environments are given: LS, IrS, Iceland basin (IcB), the eastern North Atlantic basin (ENAB) and Iberian Abyssal Plain (IAP).

4.1 Labrador Sea (stations 61 to 78)

In the LS, the HgT_{UNF} concentrations ranged from 0.25 to 0.67 pmol L^{-1} , with a mean (\pm standard deviation) of $0.44 \pm 0.10 \text{ pmol L}^{-1}$ ($n = 113$). Distribution, source and cycling of Hg in the LS have been described and discussed in detail in a companion paper (Cossa et al., 2017b). In summary, the highest HgT_{UNF} concentrations were found in the waters of the Labrador Current (LC) receiving fresh water from the Canadian Arctic Archipelago and in the waters over the Labrador shelf and continental rise. In the LSW that formed during the 2014 winter convection, HgT_{UNF} concentrations were low ($0.38 \pm 0.05 \text{ pmol L}^{-1}$, $n = 23$) and increased gradually with depth (up to $>0.5 \text{ pmol L}^{-1}$) in the North East Atlantic Deep Water.

4.2 Irminger Sea (stations 40–60)

HgT_{UNF} concentrations in the IrS waters varied from 0.22 to 0.76 pmol L^{-1} , with a mean of $0.45 \pm 0.10 \text{ pmol L}^{-1}$ ($n = 103$). In the IrSPMW, which was encountered in the upper 1000 m near eastern Greenland and the upper 500 m in the rest of the IrS (Fig. 4a in García-Ibáñez et al., 2018), HgT_{UNF} values span between 0.29 and 0.42 pmol L^{-1} (Fig. 2). Deeper HgT_{UNF} increased up to 0.50 and 0.63 pmol L^{-1} in LSW ($\sim 1000 \text{ m}$) and ISOW ($\sim 2500 \text{ m}$). Lower HgT_{UNF} concentrations ($0.40\text{--}0.50 \text{ pmol L}^{-1}$) were associated with DSOW in the bottom waters (stations 42–44, Fig. 2).

4.3 Iceland basin (stations 34–38)

HgT_{UNF} concentrations in the IcB ranged from 0.18 to 0.65 pmol L^{-1} , with a mean of $0.46 \pm 0.10 \text{ pmol L}^{-1}$ ($n = 51$). In the top 100 m of the water column, HgT_{UNF} concentrations were quite variable ($0.25\text{--}0.62 \text{ pmol L}^{-1}$), probably as a result of the counteracting importance of Hg evasion to the atmosphere, high particulate matter and/or complexing substance concentrations. West of the IcB (Station 38), contrasting HgT_{UNF} levels were found on both sides at 500 m, characterized by a thermohaline gradient (Fig. 2a and b in García-Ibáñez et al., 2018). In the top waters, HgT_{UNF} levels were depleted to 0.18 pmol L^{-1} , whereas below 500 m, they were much higher and converge to values close to what we found, at the same depths in the adjacent IrS ($\sim 0.60 \text{ pmol L}^{-1}$, Station 40). In the bottom waters, constituted by more than 50 % of ISOW (García-Ibáñez et al., 2018), HgT_{UNF} concentrations reached values $>0.50 \text{ pmol L}^{-1}$.

4.4 Eastern North Atlantic basin (stations 17–32)

The HgT_{UNF} concentrations in the ENAB varied from 0.18 to 1.14 pmol L^{-1} , with a mean of $0.61 \pm 0.18 \text{ pmol L}^{-1}$ ($n = 174$). The ENAB, also named western European basin, is characterized by complex vertical stratification of the water column. The HgT_{UNF} vertical profiles at all the stations

of the ENAB were characterized by a complex but reproducible pattern depicting (i) two maxima peaks (the upper one at the subsurface, the lower within the intermediate waters), and below, (ii) a HgT_{UNF} enhancement from 2500 m to the bottom (Fig. 2). The position and intensity of the peaks vary with longitude. The upper peak, which occurs within the top 200 m, is only 0.48 pmol L^{-1} at Station 29, but reaches 1.14 pmol L^{-1} at Station 19 (Fig. 2). The vertical position of maxima of the lower peak deepens eastwards, from 200 m down to 800 m, concurrently with an increase in its magnitude (Fig. 2). The position of the upper peaks suggests a relation with the position of the fluorescence maximum (data not shown), whereas the position of the lower peaks, which is close to the maximum of apparent oxygen utilization (AOU) that rose above $70 \mu\text{mol L}^{-1}$ (Fig. 2), suggests a dependence on the organic matter remineralization (see Discussion below). Between 1400 and 2500 m, in the layer corresponding to LSW, HgT_{UNF} concentrations were quite uniform, with a mean concentration of $0.54 \pm 0.04 \text{ pmol L}^{-1}$ ($n = 18$). The HgT_{UNF} concentration increased from 3000 m downwards to the sea bottom, consisting of NEADWL, where it reaches 0.95, 0.97, 1.03 and 1.13 pmol L^{-1} at stations 21, 19, 25 and 23, respectively.

4.5 Iberian Abyssal Plain (stations 1–15)

In the IAP, HgT_{UNF} concentrations ranged from 0.19 to 1.54 pmol L^{-1} , with a mean of $0.69 \pm 0.23 \text{ pmol L}^{-1}$ ($n = 94$). The highest HgT_{UNF} concentrations were measured in the upper 100 m near the shelf slope. At Station 2, the only station on the European shelf (bottom at 152 m), the HgT_{UNF} concentrations increased from 10 m to the bottom, from 0.38 to 0.86 pmol L^{-1} , but did not differ from the open NA ocean levels. Offshore, at stations 1, 11, 13 and 15 (Fig. 2), the vertical distributions of HgT_{UNF} presented a certain similarity with those of the eastern ENAB, but with an additional third deep peak. As in the eastern ENAB, the upper peak is associated with subsurface waters, and the second, centred around 800 m, is associated with the oxygen minimum of SPMW₈. The third peak, centred around 1100–1200 m, is associated with the salinity maximum of the core of MW (Fig. S2). The presence of a HgT_{UNF} peak in the MW was still visible westwards, at stations 17, 19 and 23, near 1100 m, as a shoulder of the main peak at 800 m (Fig. 2). Deeper within the water column, HgT_{UNF} increased gradually from 2000 m (LSW) to 3000 m (ISOW), 3500 m and below (NEADWL), where HgT_{UNF} concentrations reached 0.87 to 1.04 pmol L^{-1} depending on the station.

In summary, the HgT_{UNF} mean concentrations were low and similar in the basins of the subpolar gyre (0.44, 0.45 and 0.46 pmol L^{-1} for LS, IrS and IcB respectively), whereas they exceeded 0.60 pmol L^{-1} in the subtropical gyre (0.61 and 0.69 pmol L^{-1} for ENAB and IAP, respectively). On the other hand, the profiles were rather homogenous in the subpolar gyre compared to the multippeak vertical distribution observed in

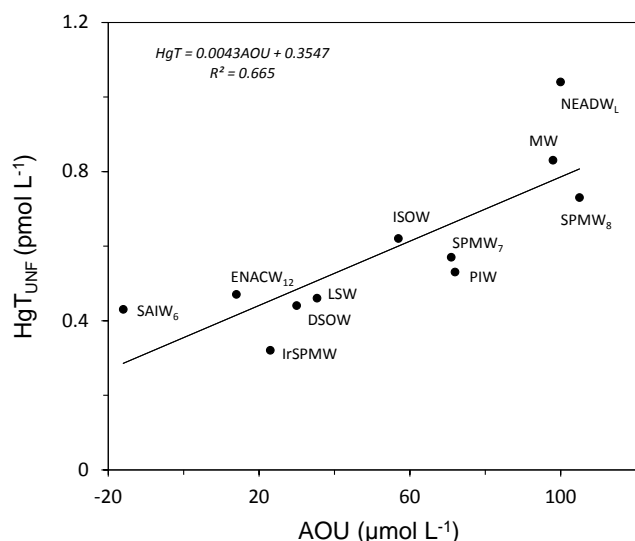


Figure 5. Total Hg in unfiltered samples (HgT_{UNF}) vs. apparent oxygen utilization (AOU) within the various source water types.

the subpolar gyre (Fig. 2). A multippeak pattern was also observed in 1994 in the eastern Atlantic slope water column in the Celtic Sea (Cossa et al., 2004). The shape of the Hg profiles exhibited the same peaks in the same water masses as the ones observed in this study (i.e. SPMWs and MW). However, HgT_{UNF} concentration levels measured 20 years ago were much higher, varying most often from 0.3 pmol L^{-1} in subsurface waters to more than 2.0 pmol L^{-1} at depth.

5 Discussion

5.1 Biogeochemical and hydrographical controls on HgT distribution

The main paths of the Hg cycle in the open ocean can be briefly summarized as follows. Direct atmospheric deposition is the dominant source of Hg for the oceans, most of the deposited Hg is re-emitted in the atmosphere, and a minor Hg fraction is drawn down to the ocean interior with downwards convecting waters or associated with sinking particles. At depth, the dissolution of particulate matter, produced as a result of organic matter microbiological remineralization, remobilizes Hg from particles produced in the euphotic zone. The biological pumping/regeneration process results in a relationship between Hg concentrations and nutrient or dissolved oxygen concentration (or AOU), which are proxies of the organic matter remineralization (mainly the microbial respiration) that the sample had experienced since it was last in contact with the atmosphere. This biogeochemical behaviour, which is qualified of nutrient-like behaviour, is observed in the present study (Fig. 4). The correlation coefficient (R) between HgT_{F} and the AOU, obtained from in situ measurements of dissolved oxygen and temperature, reached

the highly statistically significant value of 0.87 ($n = 141$, $p < 0.01$). Similar behaviour was already observed in the water column near the shelf edge of the western European margin (Cossa et al., 2004) and elsewhere in the NA (Lamborg et al., 2014; Bowman et al., 2015). Thus, the present results confirm that biological uptake and regenerative processes appear to control a large part of the oceanic Hg distribution in the subpolar and subtropical gyres of the NA.

Hydrological circulation may also impact the Hg distribution in the NA. We estimated the HgT_{UNF} (and AOU) values of each SWT using eOMP (Table 1). The correlation coefficient between observed and predicted (eOMP-based) values calculated with Eq. (1) (Materials and Methods section) for HgT_{UNF} is 0.71 . The estimated HgT_{UNF} concentrations vary significantly between SWTs from 0.32 ± 0.03 to $1.04 \pm 0.02 \text{ pmol L}^{-1}$ for the IrSPM to the NEADW_L. However, a large part of the HgT_{UNF} between SWTs is due to the regeneration process as suggested by the correlation coefficient ($R = 0.82$) of the linear relationship between HgT_{UNF} and AOU (Fig. 5). Based on this model ($\text{HgT}_{\text{UNF}} = 0.0043 \times \text{AOU} + 0.3547$), we calculated mean corrected HgT_{UNF} concentrations for each identified SWT for a zero AOU concentration. Corrected mean values range from 0.22 to 0.61 pmol L^{-1} in IrSPMW and NEADW, respectively (Table 1). This variation should result from the origin, the route and the age of each SWT. The corrected HgT_{UNF} values of IrSPMW, PIM, SPMW, DSOW and LSW, which formed in the subpolar gyre and in the NS last winter, present very low and similar values, 0.22 – 0.31 (Table 1). The IrSPMW is the youngest SPMW that has formed in the IrS as a result of interaction between the air and the waters transported northwards by the NAC (e.g. McCartney and Talley, 1984); the low HgT_{UNF} value found in the IrSPMW may result from a net Hg evasion in this region, consistently with the conclusion that western and central NA are a net source of Hg in the atmosphere (Mason et al., 2017). On the contrary, on the eastern NA side, where Hg deposition and evasion are rather similar (Mason et al., 2017), the ENACW shows a higher corrected HgT concentration (0.41 pmol L^{-1} , Table 1). The highest corrected HgT_{UNF} mean concentration is calculated for NEADW_L (0.61 pmol L^{-1} , Table 1), which is the dominant water mass in the bottom IAP. Its main core is below $\sim 3500 \text{ m}$ depth and spreads down to the bottom (see Fig. 4 in García-Ibáñez et al., 2018). This water mass contains a significant component from the Southern Ocean (AABW), which is known to be Hg-rich ($\text{HgT}_{\text{AABW}} = 1.35 \pm 0.39 \text{ pmol L}^{-1}$, Cossa et al., 2011). The same rationale can be drawn for the corrected HgT_{UNF} concentration in MW (0.41 pmol L^{-1} , Table 1). Indeed, recent measurements in the waters of the western Mediterranean give HgT_{UNF} values between 0.53 and 1.25 pmol L^{-1} within the layer that flows out of the Mediterranean Sea at the Strait of Gibraltar (Cossa and Coquery, 2005; Cossa et al., 2017a).

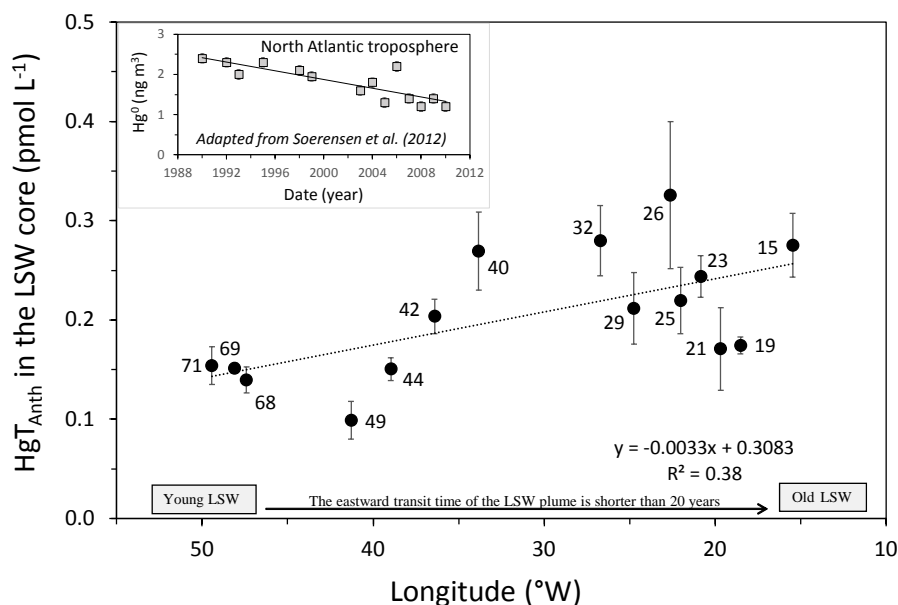


Figure 6. Anthropogenic HgT_{Anth} concentration distribution in the core of the Labrador Sea Water (LSW) ($S = 34.9$, $\sigma_{\text{O}} = 27.74\text{--}27.82$, 1200–2000 m) between the Labrador Sea and the eastern North Atlantic basin. HgT_{Anth} values were obtained according to the model by Lamborg et al. (2014). Young LSW corresponds to the LSW₂₀₁₄ formed during winter 2013–2014. The insert shows the Hg concentration decrease in the troposphere over the North Atlantic during the last 20 years according to Soerensen et al. (2012).

Table 1. Total Hg in unfiltered samples (HgT_{UNF}) vs. apparent oxygen utilization (AOU) concentrations of each source water type (SWT), calculated according to eOMP (Eq. 1) (see also García-Ibáñez et al., 2018). Corrected HgT_{UNF} is a theoretical HgT concentration for a AOU concentration equal to zero, using the equation from Fig. 5. ENACW₁₂: eastern North Atlantic Central Water of 12 °C; SPMW₈ and SPMW₇: Subpolar Mode Water of the Iceland basin of 7 and 8 °C; IrSPMW: Subpolar Mode Water of the Irminger basin; LSW: Labrador Sea Water; MW: Mediterranean waters; ISOW: Iceland–Scotland Overflow Water; NEADW_L: Lower North East Atlantic Deep Water; DSOW: Denmark Strait Overflow Water; PIW: Polar Intermediate Water; and SAIW₆: Subarctic Intermediate Water of 6 °C.

SWT	HgT_{UNF} (pmol L^{-1})	AOU ($\mu\text{mol L}^{-1}$)	Corrected HgT_{UNF} (pmol L^{-1})
ENACW ₁₂	0.47 ± 0.01	14 ± 2	0.41
SPMW ₈	0.73 ± 0.03	105 ± 4	0.28
SPMW ₇	0.57 ± 0.03	71 ± 3	0.27
IrSPMW	0.32 ± 0.03	23 ± 4	0.22
SAIW ₆	0.43 ± 0.03	-16 ± 4	0.50
MW	0.83 ± 0.05	98 ± 5	0.41
LSW	0.46 ± 0.01	35 ± 1	0.31
NEADW _L	1.04 ± 0.02	100 ± 2	0.61
PIW	0.53 ± 0.10	72 ± 11	0.22
ISOW	0.62 ± 0.02	57 ± 2	0.38
DSOW	0.44 ± 0.03	30 ± 4	0.31

In summary, the distribution pattern of HgT_{UNF} along the GEOTRACES-GA01 transect, modelled by the mixing of SWTs (Fig. S4), stresses the importance of Hg scavenging by plankton and organic matter regeneration, but also shows that part of the Hg enrichment in certain SWTs, including MW and NEADW, is due to preformed Hg outside the NA. This type of result, characterizing the Hg concentrations in

principal oceanic water masses, should contribute to refinements in model formulation and predictability.

5.2 Change in anthropogenic Hg in LSW

Evidence for a decrease in the Hg anthropization in the NA waters can be obtained from the comparison of the present results with those obtained 20 years ago with similar clean sampling and analytical techniques. In a companion paper

Table 2. Water and total Hg in unfiltered samples (HgT_{UNF}) transported by the upper and lower limbs of the Atlantic Meridional Overturning Circulation. Positive (negative) transport corresponds to northward (southward) flow.

SWT	Entire water column		Upper limb		Lower limb	
	Water transport (Sv)	HgT_{UNF} transport (mmol s^{-1})	Water transport (Sv)	HgT_{UNF} transport (mmol s^{-1})	Water transport (Sv)	HgT_{UNF} transport (mmol s^{-1})
ENACW ₁₂	9.5	4.52	9.5	4.52	0.0	0.00
SPMW ₈	4.1	3.02	3.7	2.70	0.4	0.31
SPMW ₇	3.3	1.86	1.8	1.01	1.5	0.85
IrSPMW	-10.2	-3.23	-0.6	-0.19	-9.6	-3.04
SAIW ₆	1.0	0.41	2.4	1.04	-1.5	-0.62
MW	0.7	0.60	0.6	0.53	0.1	0.06
LSW	1.9	0.87	1.4	0.86	0.5	0.21
NEADW _L	0.3	0.34	0.0	0.00	0.3 ₃	0.34
PIW	-2.2	-1.18	-0.1	-0.08	-2.1	-1.10
ISOW	-4.9	-3.04	0.0	0.00	-4.9	-3.04
DSOW	-2.5	-1.09	0.0	0.00	-2.5	-1.09
Total	1.1	3.08	18.7	10.2	-17.7	-7.12

(Cossa et al., 2017b), we have already compared the present findings for the convection layer in the LS with the results of the 1993 International Oceanographic Commission cruise (Mason et al., 1998). Between 1993 and 2014 the decrease in HgT_{UNF} concentrations would have been more than a factor of 2 ($1.14 \pm 0.36 \text{ pmol L}^{-1}$ vs. $0.40 \pm 0.07 \text{ pmol L}^{-1}$). However, bearing in mind the uncertainty of the accuracy of early numbers, this magnitude of decrease cannot be taken for granted. To circumvent this difficulty, the approach proposed by Lamborg et al. (2014) can be used to estimate the anthropogenic Hg (Hg_{Anth}) concentrations in subsurface waters. Hg_{Anth} is inferred from the difference between measured HgT_{UNF} concentrations and the concentrations predicted based on a worldwide relationship between deep-ocean Hg concentrations and remineralised phosphate (Lamborg et al., 2014). There is a Redfield ratio of 141 between AOU and remineralized phosphate (Minster and Boulaïdid, 1987), which is more representative for the NA than the global value of 170 proposed by Anderson and Sarmiento (1994). The LSW takes less than 20 years (Doney et al., 1997) to flow more than 3000 km eastward from the LS to the subtropical gyre of the NA. Along its path, LSW bears the record of Hg incorporation at the time of its formation; thus sampling along its flow path allows the observation of decadal variations in anthropogenic Hg inputs to the NA. In the NA, estimation of Hg_{Anth} concentrations in the core of LSW, defined within potential densities of 27.74 and 27.82, account for $36 \pm 0.07 \%$ of the HgT_{UNF} , and are one-third lower for younger waters (LS and IrS: $0.16 \pm 0.11 \text{ pM}$) than for older waters (IcB and ENAB: $0.24 \pm 0.06 \text{ pM}$) (Fig. 6). This 30 % decrease in Hg concentrations are consistent (i) with the observations of a temporal decrease of Hg in the marine boundary layer of the NA (Sprovieri et al., 2010; Weigelt et al.,

2014) over the last two decades and with (ii) the estimated decline in Hg concentrations in subsurface waters of the NA estimated by models over the last few decades (e.g. Sorensen et al., 2012).

This means that LSW that formed in the 1990s in the LS and is currently present in the ENAB received more Hg_{Anth} from the atmosphere than the LSW_{2014–2015} that formed during the 2014 winter. These results contrast with what can be deduced from the vertical profile of HgT_{UNF} in the LS, where the Hg regeneration in the water column is sufficient to account for the Hg increase between the shallow LSW layer (LSW_{2014–2015}) and the deep LSW layer (LSW_{1987–1994}) (Cossa et al., 2017b). This discrepancy between these two deductions suggests that LSW, which is present in the eastern NA, is likely older (and more imprinted by legacy Hg_{Anth}) than the LSW currently present in the LS.

5.3 Latitudinal transport of Hg

The transport of HgT_{UNF} per unit of water mass, calculated with Eq. (2) (Materials and Methods section), are given in Table 2. We also applied Eq. (2) separately to the upper and lower limbs of the AMOC and computed the transport of HgT_{UNF} per water mass for the two limbs. The velocity fields across the Portugal–Greenland transect were calculated using an inverse model constrained by Doppler current profiler velocity measurements (Zunino et al., 2017). The volume transport per SWT was computed by combining these velocity fields with the results of the eOMP (García-Ibáñez et al., 2018).

The mean (velocity-weighted) HgT_{UNF} concentration of the water advected northwards within the upper limb of the AMOC is 0.55 pmol L^{-1} , whereas the one advected south-

wards within the lower limb of the AMOC is 0.40 pmol L^{-1} . Across the Portugal–Greenland transect, there is northward HgT_{UNF} transport within the upper limb of the AMOC ($10.20 \text{ mmol s}^{-1}$), and southward HgT_{UNF} transport within the lower limb (7.12 mmol s^{-1}), resulting in a net northward transport of $97.2 \text{ kmol yr}^{-1}$. Most of the HgT_{UNF} southward transport is due to IrSPMW and ISOW displacements, whereas the HgT_{UNF} northward transport is associated with ENACW and SPMW displacements (Table 2). The Hg exchange across the LS section can be roughly estimated at 133 kmol yr^{-1} , using the mean southward water transport of the shelf edge LC as the Seal Island transect (Hamilton Bank near stations 77 and 78; 7.5 Sv , according to Han et al., 2008) and a mean HgT concentration of 0.56 pmol L^{-1} (Cossa et al., 2017b). Thus, from our snapshot study, the net Hg exchange across the GEOVIDE transect, which crosses the LS and the NA from Portugal and Greenland, would mean a loss in the Arctic of 36 kmol yr^{-1} . In comparison, Soerensen et al. (2016), based on a mass balance budget, estimated that “Arctic seawater is enriched in total Hg relative to inflowing waters from the North Atlantic and North Pacific Oceans at all depths, resulting in a 26 Mg a^{-1} (i.e. 130 kmol a^{-1}) net loss from the Arctic via circulation”.

6 Summary and conclusions

HgT_{UNF} concentrations in the waters along the GEOTRACES-GA01 transect, which crossed the NA from 40 to 60° N (Portugal to Canada), ranged from 0.16 to 1.54 pmol L^{-1} , but with 97% of the values lower than 1.00 pmol L^{-1} and a geometric mean of 0.51 pmol L^{-1} ($n = 535$). The dissolved fraction ($<0.45 \mu\text{m}$) of HgT , determined on 141 samples, averaged 78% of the HgT_{UNF} for the entire data set, 84% for deep open seawaters and 91% if the Labrador Sea data, where the primary production was high, are excluded. HgT_{UNF} concentrations increased eastwards and downwards. The HgT_{UNF} concentrations were similarly low in the sub-polar gyre waters ($\sim 0.45 \text{ pmol L}^{-1}$), whereas they exceeded 0.60 pmol L^{-1} in the subtropical gyre waters, especially within NEADW_L. The relationship between HgT_{F} and AOU, which indicates a nutrient-like behaviour for Hg in the NA, attests to the influence of organic matter regeneration on HgT mobilization. The distribution pattern of HgT_{UNF} along the transect, modelled by the mixing of SWTs, show Hg enrichment in MW and NEADW, and low Hg concentrations in younger water masses that formed last winter at high latitudes. Using the HgT_{UNF} fraction unexplained by regeneration processes as a proxy for Hg_{Anth} , we observed geographical trend in the Hg_{Anth} in the LSW along its eastward journey in the NA. It was characterized by an eastward increase, which suggests that Hg incorporation in the downwelling waters of the LS has decreased over the last 20 years, parallel with the decrease in Hg concentrations in the NA troposphere. By combining the velocity fields with the results

of the eOMP, a net northward Hg transfer of $97.2 \text{ kmol yr}^{-1}$ across the Portugal–Greenland transect can be calculated as a result of the AMOC. Taking into account the southern Hg export with the LC, the net Hg exchange along the entire GEOVIDE transect would result in a loss in the Arctic of 36 kmol yr^{-1} .

Data availability. The data are available at the website: www.eGEOTRACES.org.

Appendix A

Abbreviations

AABW	Antarctic Bottom Water
AFS	Atomic fluorescence spectrometer
AMOC	Atlantic Meridional Overturning Circulation
AOU	Apparent oxygen utilization
CFCs	Chlorofluorocarbons
CRM	Certified reference material
DL	Detection limit
DSOW	Denmark Strait Overflow Water
DWBC	Deep Western Boundary Current
EGC	East Greenland Current
ENAB	Eastern North Atlantic basin
ENACW	Eastern North Atlantic Central Water
eOMP	Extended optimum multiparameter analysis
Hg	Mercury
HgT _{Anth}	anthropogenic HgT
HgT	Total mercury
HgT _{UNF}	unfiltered HgT
HgT _F	filtered HgT
IAP	Iberian Abyssal Plain
IcB	Iceland basin
IOC	International Oceanographic Commission
IrS	Irminger Sea
ISOW	Iceland–Scotland Overflow Water
LC	Labrador Current
LS	Labrador Sea
LSW	Labrador Sea Water
MW	Mediterranean waters
NA	North Atlantic Ocean
NAC	North Atlantic Current
NADW	North Atlantic Deep Water
NEADW _L	Lower North East Atlantic Deep Water
PIW	Polar Intermediate Water
SPMW	Subpolar Mode Water
SWT	Source water type
WGC	West Greenland Current

The Supplement related to this article is available online at <https://doi.org/10.5194/bg-15-2309-2018-supplement>.

Competing interests. The authors declare that they have no conflict of interest.

Special issue statement. This article is part of the special issue “GEOVIDE, an international GEOTRACES study along the OVIDE section in the North Atlantic and in the Labrador Sea (GA01)”. It is not associated with a conference.

Acknowledgements. Thanks are due to members of the GEOVIDE team for participating in data acquisition: Fernando Alonso Pérez, Ryan Barkhouse, Vincent Bouvier, Pierre Branellac, Lidia Carracedo Segade, Maxi Castrillejo, Leonardo Contreira, Nathalie Deniault, Floriane Desprez de Gesincourt, Lorna Foliot, Debany Fonseca Pereira, Emilie Grossteffan, Pierre Hamon, Catherine Jeandel, Catherine Kermabon, François Lacan, Philippe Le Bot, Manon Le Goff, Alison Lefebvre, Stéphane Leizour, Nolwen Lemaitre, Olivier Menage, Frédéric Planchon, Arnout Roukaerts, Virginie Sanial, Raphaëlle Sauzède, and Yi Tang. A special thank you is also due to the R/V “*Pourquoi Pas?*” crew and Captain Gilles Ferrand, and the DT INSU (Emmanuel de Saint-Léger, Fabien Pérault), who organized the rosette deployment/recovery processes. This research was funded by the French National Research Agency (ANR-13-BS06-0014, ANR-12-PDOC-0025-01), the French National Center for Scientific Research (CNRS-LEFE-CYBER), the LabexMER (ANR-10-LABX-19), the Global Mercury Observation System (GMOS, no. 265113 European Union project), and the European Research Council (ERC-2010-StG-20091028). For this work Maribel I. García-Ibáñez and Fiz F. Pérez were supported by the Spanish Ministry of Economy and Competitiveness through the BOCATS (CTM2013-41048-P) project, co-funded by the Fondo Europeo de Desarrollo Regional 2014–2020 (FEDER).

Edited by: Catherine Jeandel

Reviewed by: two anonymous referees

References

- Amos, H. M., J. E. Sonke, J. E., Obrist, D., Robins, N., Hagan, N., Horowitz, H. M., Mason, R. P., Witt, M., Hedgecock, I. M., Corbitt, E. S., and Sunderland, E. M.: Observational and Modeling Constraints on Global Anthropogenic Enrichment of Mercury, *Environ. Sci. Technol.*, 49, 4036–4047, 2015.
- Amyot, M., Gill, G. A., and Morel, F. M. M.: Production and loss of dissolved gaseous mercury in coastal seawater, *Environ. Sci. Technol.*, 31, 3606–3611, 1997.
- Anderson, L. A. and Sarmiento, J. L.: Redfield ratios of remineralization determined by nutrient data-analysis, *Global Biogeochem. Cy.*, 8, 65–80, 1994.
- Bloom, N. S. and Crecelius, E. A.: Determination of mercury in seawater at sub-nanogram per liter levels, *Mar. Chem.*, 14, 49–59, [https://doi.org/10.1016/0304-4203\(83\)90069-5](https://doi.org/10.1016/0304-4203(83)90069-5), 1985.
- Bowman, K. L., Hammerschmidt, C. R., Lamborg, C. H., and Swarr, G. J.: Mercury in the North Atlantic Ocean: The U.S. GEOTRACES zonal and meridional, Deep-Sea Res. Pt. II, 116, 251–261, <https://doi.org/10.1016/j.dsr2.2014.07.004>, 2015.
- Bowman, K. L., Hammerschmidt, C. R., Lamborg, C. H., Swarr, G. J., and Agather, A. M.: Distribution of mercury species across a zonal section of the eastern tropical South Pacific Ocean (US GEOTRACES GP16), *Mar. Chem.*, 186, 156–166, 2016.
- Brambilla, E. and Talley, L. D.: Subpolar Mode Water in the northeastern Atlantic: 1. Averaged properties and mean circulation, *J. Geophys. Res.-Ocean.*, 113, C04025, <https://doi.org/10.1029/2006JC004062>, 2008.
- Bratkich, A., Vahčić, M., Kotnik, J., Obu Vazner, K., Begu, E., Woodward, E. M. S., and Horvat, M.: Mercury presence and speciation in the South Atlantic Ocean along the 40° S transect, *Global Biogeochem. Cy.*, 30, 105–119, <https://doi.org/10.1002/2015GB005275>, 2016.
- Cianca A., Santana, R., Marrero, J. P., Rueda, M. J., and Llina, O.: Modal composition of the central water in the North Atlantic subtropical gyre, *Ocean Sci. Discuss.*, 6, 2487–2506, <https://doi.org/10.5194/osd-6-2487-2009>, 2009.
- Cossa, D. and Coquery, M.: The Mediterranean mercury anomaly, a geochemical or a biological issue, in: *The Mediterranean Sea, Handbook of Environmental Chemistry*, edited by: Saliot, A., Springer, ISSN 1433-6863, Vol. 5, 177–208, 2005.
- Cossa, D. and Courau, P.: An international intercomparison exercise for total mercury in seawater, *Appl. Organometal. Chem.*, 4, 49–54, <https://doi.org/10.1002/aoc.590040109>, 1990.
- Cossa, D., Cotté-Krief, M.-H., Mason, R. P., and Bretaudeau-Sanjuan, J.: Total mercury in the water column near the shelf edge of the European continental margin, *Mar. Chem.*, 90, 21–29, <https://doi.org/10.1016/j.marchem.2004.02.019>, 2004.
- Cossa, D., Heimbürger, L.-E., Lannuzel, D., Rintoul, S. R., Butler, E. C. V., Bowie, A. R., Averty, B., Watson, R. J., and Remenyi, T.: Mercury in the Southern Ocean, *Geochim. Cosmochim. Ac.*, 7, 4037–4052, <https://doi.org/10.1016/j.gca.2011.05.001>, 2011.
- Cossa, D., Durrieu de Madron, X., Schäfer, J., Guédron, S., Maruszczak, N., Castelle, S., and Naudin, J.-J.: Sources and exchanges of mercury in the waters of the Northwestern Mediterranean margin, *Prog. Oceanogr.*, <https://doi.org/10.1016/j.pocean.2017.05.002>, 2017a.
- Cossa, D., L.-E. Heimbürger, L.-E., Sonke, J. E., Planquette, H., Lherminier, P., García-Ibáñez, M. I., Pérez, F. F., and Sarthou, G.: Sources, recycling and transfer of mercury in the Labrador Sea (GEOTRACES-GEOVIDE cruise), *Mar. Chem.*, 198, 64–69, <https://doi.org/10.1016/j.marchem.2017.11.006>, 2017b.
- Cutter, G., Casciotti, K., Croot, P., Geibert, W., Heimbürger, L. E., Lohan, M., Planquette, H., and van de Fliert, T.: GEOTRACES cookbook: Sampling and sample-handling protocols for GEOTRACES cruises, Version 3, the 2017 GEOTRACES Standards and Intercalibration Committee, Version 3.0, August 2017.
- Cutter, G. A. and Bruland, K. W.: Rapid and noncontaminating sampling system for trace elements in global ocean surveys, *Limnol. Oceanogr.-Method.*, 10, 425–436, <https://doi.org/10.4319/lom.2012.10.425>, 2012.

- Daniault, N., Lherminier, P., and Mercier, H.: Circulation and transport at the southeast tip of Greenland, *J. Phys. Oceanogr.*, 41, 437–457, <https://doi.org/10.1175/2010JPO4428.1>, 2011.
- Daniault, N., Mercier, H., Lherminier, P., Sarafanov, A., Falina, A., Zunino, P., Pérez, F. F., Ríos, A. F., Ferron, B., Huck, T., Thierry, V., and Gladyshev, S.: The northern North Atlantic Ocean mean circulation in the early 21st century, *Progr. Oceanogr.*, 146, 142–158, <https://doi.org/10.1016/j.pocean.2016.06.007>, 2016.
- de la Paz, M., García-Ibáñez, M. I., Steinfeldt, R., Ríos, A. F., and Pérez F. F.: Ventilation versus biology: What is the controlling mechanism of nitrous oxide distribution in the North Atlantic?, *Global Biogeochem. Cy.*, 31, 745–760, <https://doi.org/10.1002/2016GB005507>, 2017.
- Doney, S. C., Jenkins, W. J., and Bullister, J. L.: A comparison of ocean tracer dating techniques on a meridional section in the eastern North Atlantic, *Deep-Sea Res. Pt. I*, 44, 603–626, 1997.
- EPA (Environmental Protection Agency, US): Method 1631, Revision E: Mercury in water by oxidation, purge and trap, and cold vapor atomic fluorescence spectrometry, EPA-821-R-02-019, <http://water.epa.gov/scitech/methods/cwa/metals/mercury/index.cfm>, 2002.
- Fitzgerald, W. F., Lamborg, C. H., and Hammerschmidt, C. R.: Marine biogeochemical cycling of mercury, *Chem. Rev.*, 107, 641–662, 2007.
- Fontela, M., García-Ibáñez, M. I., Hansell, D. A., Mercier, H., and Pérez, F. F.: Dissolved Organic Carbon in the North Atlantic Meridional Overturning Circulation, *Sci. Rep.*, 6, 26931, <https://doi.org/10.1038/srep26931>, 2016.
- García-Ibáñez, M. I., Pardo, P. C., Carracedo, L. I., Mercier, H., Lherminier, P., Ríos, A. F., and Pérez, F. F.: Structure, transports and transformations of the water masses in the Atlantic Subpolar Gyre, *Prog. Oceanogr.*, 135, 18–36, <https://doi.org/10.1016/j.pocean.2015.03.009>, 2015.
- García-Ibáñez, M. I., Pérez, F. F., Lherminier, P., Zunino, P., and Treguer, P.: Water mass distributions and transports for the 2014 GEOVIDE cruise in the North Atlantic, *Biogeosciences*, 15, 2075–2090, <https://doi.org/10.5194/bg-15-2075-2018>, 2018.
- Gill, G. A. and Fitzgerald, W. F.: Mercury sampling of open ocean waters at the picomolar level, *Deep-Sea Res. Pt. A*, 32, 287–297, [https://doi.org/10.1016/0198-0149\(85\)90080-9](https://doi.org/10.1016/0198-0149(85)90080-9), 1985.
- Gill, G. A. and Fitzgerald, W. F.: Vertical mercury distributions in the oceans, *Geochim. Cosmochim. Ac.*, 53, 1719–1728, 1988.
- Gourcuff, C., Lherminier, P., Mercier, H., and Le Traon, P. Y.: Altimetry combined with hydrography for ocean transport estimation, *J. Atmos. Oceanogr. Technol.*, 28, 1324–1337, <https://doi.org/10.1175/2011JTECHO818.1>, 2011.
- Han, G., Lu, Z., Wang, Z., Helbig, J., Chen, N., and de Young, B.: Seasonal variability of the Labrador Current and shelf circulation off Newfoundland, *J. Geophys. Res.*, 113, C10013, <https://doi.org/10.1029/2007JC004376>, 2008.
- Heimbürger, L.-E., Sonke, J., Cossa, D., Point, D., Lagane, C., Laffont, L., Galfond, B. T., Nicolaus, M., Rabe, B., and Rutgers van der Loeff, M.: Shallow methylmercury production in the marginal sea ice zone of the central Arctic Ocean, *Sci. Rep.*, 5, 10318, <https://doi.org/10.1038/srep10318>, 2015.
- Hewitt, C. N.: Instrumental Analysis of Pollutants, Elsevier Applied Science, 1989.
- Kuhlbrodt, T., Griesel, A., Montoya, M., Levermann, A., Hofmann, M., and Rahmstorf, S.: On the driving processes of the Atlantic meridional overturning circulation, *Atlantic*, 45, RG2001, <https://doi.org/10.1029/2004RG000166>, 2007.
- Lamborg, C. H., Hammerschmidt, C. R., Gill, G. A., Mason, R. P., and Gichuki, S.: An intercomparison of procedures for the determination of total mercury in seawater and recommendations regarding mercury speciation during GEO-TRACES cruises, *Limnol. Oceanogr.-Method.*, 10, 90–100, <https://doi.org/10.4319/lom.2012.10.90>, 2012.
- Lamborg, C. H., Hammerschmidt C. R., Bowman, K. L., Swarr, G. J., Munson, K. M., Ohnemus, D. C., Lam, P. J., Heimbürger, L.-E., Rijkenberg, M. J. A., and Saito, M. A.: A global ocean inventory of anthropogenic mercury based on water column measurements, *Nature*, 512, 65–68, <https://doi.org/10.1038/nature13563>, 2014.
- Lemaitre, N., Planquette, H., Planchon, F., Sarthou, G., Jacquet, S., García-Ibáñez, M. I., Gourain, A., Cheize, M., Monin, L., André, L., Laha, P., Terryn, H., and Dehairs, F.: Particulate barium tracing significant mesopelagic carbon remineralisation in the North Atlantic, *Biogeosciences Discuss.*, <https://doi.org/10.5194/bg-2017-400>, in review, 2017.
- Lherminier, P., Mercier, H., Gourcuff, C., Álvarez, M. F., Bacon, S., and Kermabon, C.: Transport across the 2002 Greenland-Portugal section and comparison with 1997, *J. Geophys. Res.*, 112, C07003, <https://doi.org/10.1029/2006JC003716>, 2007.
- Lherminier, P., Mercier, H., Huck, T., Gourcuff, C., Pérez, F. F., Morin, P., Sarafanov, A., and Falina, A.: The Atlantic Meridional Overturning Circulation and the Subpolar Gyre observed at the A25-OVIDE Section in June 2002 and 2004, *Deep-Sea Res. Pt. I*, 57, 1374–1391, <https://doi.org/10.1016/j.dsr.2010.07.009>, 2010.
- Mason, R. P. and Fitzgerald, W. F.: The distribution and biogeochemical cycling of mercury in the equatorial Pacific Ocean, *Deep-Sea Res. Pt. I*, 40, 1897–1924, 1993.
- Mason, R. P. and Sheu, G.-R. : Role of the ocean in the global mercury cycle, *Global Biogeochem. Cy.*, 16, 1093, <https://doi.org/10.1029/2001GB001440>, 2002.
- Mason, R. P., Fitzgerald, W. F., and Morel, F. M. M.: The biogeochemical cycling of elemental mercury: Anthropogenic influences, *Geochim. Cosmochim. Ac.*, 58, 3191–3198, 1994.
- Mason, R. P., Morel, F. M. M., and Hemond, H. F.: The role of microorganisms in elemental mercury formation in natural waters, *Water Air Soil Poll.*, 80, 775–787, 1995.
- Mason R. P., Rolfus K. R., and Fitzgerald W. F.: Mercury in the North Atlantic, *Mar. Chem.*, 61, 37–53, [https://doi.org/10.1016/S0304-4203\(98\)00006-1](https://doi.org/10.1016/S0304-4203(98)00006-1), 1998.
- Mason, R. P., Choi, A. L., Fitzgerald, W. F., Hammerschmidt, C. R., Lamborg, C. H., Soerensen, A. L., and Sunderland, E. M.: Mercury biogeochemical cycling in the ocean and policy implications, *Environ. Res.*, 119, 101–117, 2012.
- Mason, R. P., Hammerschmidt, C. R., Lamborg, C. H., Bowman, K. L., Swarr, G. J., and Shelley, R. U.: The air-sea exchange of mercury in the low latitude Pacific and Atlantic Oceans, *Deep-Sea Res. Pt. I*, 122, 17–28, <https://doi.org/10.1016/j.dsr.2017.01.015>, 2017.
- McCartney, M. S.: Recirculating components to the deep boundary current of the northern North Atlantic, *Prog. Oceanogr.*, 29, 283–383, [https://doi.org/10.1016/0079-6611\(92\)90006-L](https://doi.org/10.1016/0079-6611(92)90006-L), 1992.
- McCartney, M. S. and Talley, L. D.: The subpolar mode water of the North Atlantic Ocean, *J. Phys.*

- Oceanogr., 12, 1169–1188, [https://doi.org/10.1175/1520-0485\(1982\)012<1169:TSMWOT>2.0.CO;2](https://doi.org/10.1175/1520-0485(1982)012<1169:TSMWOT>2.0.CO;2), 1982.
- McCartney, M. S. and Talley, L. D.: Warm-to-cold conversion in the northern North Atlantic Ocean, *J. Phys. Oceanogr.*, 14, 922–935, [https://doi.org/10.1175/1520-0485\(1984\)014<0922:WTCWCI>2.0.CO;2](https://doi.org/10.1175/1520-0485(1984)014<0922:WTCWCI>2.0.CO;2), 1984.
- Mercier, H., Lherminier, P., Sarafanov, A., Gaillard, F., Daniault, N., Desbruyères, D., Falina, A., Ferron, B., Gourcuff, C., Huck, T., and Thierry, V.: Variability of the meridional overturning circulation at the Greenland-Portugal OVIDE section from 1993 to 2010, *Prog. Oceanogr.*, 132, 250–261, <https://doi.org/10.1016/j.pocean.2013.11.001>, 2015.
- Minster, J.-F. and Boulahdid, M.: Redfield ratios along isopycnal surfaces – a complementary study, *Deep-Sea Res. Pt. I*, 34, 1981–2003, 1987.
- Munson, K. M., Lamborg, C. H., Swarr, G. J., and Saito, M. A.: Mercury species concentrations and fluxes in the Central Tropical Pacific Ocean, *Global Biogeochem. Cy.*, 29, 656–676, <https://doi.org/10.1002/2015GB005120>, 2015.
- Rhein, M., Fisher, J., Smethie, W. M., Smythe-Wright, D., Weiss, R. F., Mertens, C., Min, D.-H., Fleischmann, U., and Putzka, A.: Labrador Sea water: Pathways, CFC Inventory, and Formation Rates, *J. Phys. Oceanogr.*, 32, 648–665, [https://doi.org/10.1175/1520-0485\(2002\)032<0648:LSWPCI>2.0.CO;2](https://doi.org/10.1175/1520-0485(2002)032<0648:LSWPCI>2.0.CO;2), 2002.
- Soerensen, A. L., Jacob, D. J., Streets, D. G., Witt, M. L. I., Ebinghaus, R., Mason, R. P., Andersson, M., and Sunderland, E. M.: Multi-decadal decline of mercury in the North Atlantic atmosphere explained by changing subsurface seawater concentrations, *Geophys. Res. Lett.*, 39, L21810, <https://doi.org/10.1029/2012GL053736>, 2012.
- Soerensen, A. L., Jacob, D. J., Schartup, A. T., Fisher, J. A., Lehnher, I., St. Louis, V. L., Heimbürger, L. E., Sonke, J. E., Krabbenhoft, D. P., and Sunderland, E. M.: A mass budget for mercury and methylmercury in the Arctic Ocean, *Global Biogeochem. Cy.*, 30, 560–575, <https://doi.org/10.1002/2015GB005280>, 2016.
- Sprovieri, F., Pirrone, N., Ebinghaus, R., Kock, H., and Dommergue, A.: A review of worldwide atmospheric mercury measurements, *Atmos. Chem. Phys.*, 10, 8245–8265, <https://doi.org/10.5194/acp-10-8245-2010>, 2010.
- Taylor, J. K.: *Quality Assurance of Chemical Measurements*, Lewis Publishers, 1987.
- Tsuchiya, M., Talley, L. D., and McCartney, M. S.: An eastern Atlantic section from Iceland southward across the equator, *Deep-Sea Res. Pt. A*, 39, 1885–1917, [https://doi.org/10.1016/0198-0149\(92\)90004-D](https://doi.org/10.1016/0198-0149(92)90004-D), 1992.
- van Aken, H. M. and Becker, G.: Hydrography and through-flow in the northeastern North Atlantic Ocean: the NANSEN project, *Prog. Oceanogr.*, 38, 297–346, [https://doi.org/10.1016/S0079-6611\(97\)00005-0](https://doi.org/10.1016/S0079-6611(97)00005-0), 1996.
- Weigelt, A., Ebinghaus, R., Manning, A. J., Derwent, R. G., Simmonds, P. G., Spain, T. G., Jennings, S. G., and Slemr, F.: Analysis and Interpretation of 18 years of mercury observations since 1996 at Mace Head, Ireland, *Atmos. Environ.*, 100, 85–93, <https://doi.org/10.1016/j.atmosenv.2014.10.050>, 2014.
- Yashayaev, I. and Loder, J. W.: Recurrent replenishment of Labrador Sea Water and associated decadal-scale variability, *J. Geophys. Res.-Ocean.*, 121, 8095–8114, <https://doi.org/10.1002/2016JC012046>, 2016.
- Yashayaev, I., Head, E.J.H., Azetsu-Smith, K., Ringuette, M., Wang, Z., Anning, J., and Punshon, S.: Environmental Conditions in the Labrador Sea during 2014, Northwest Atlantic Fisheries Organization, Scientific Council Meeting (June 2015), Serial No. N6436, NAFO SCR Doc. 15/015, 33 pp., 2015.
- Zhang, Y., Jaeglé, L., and Thompson, L. A.: Natural biogeochemical cycle of mercury in a global three-dimensional ocean tracer model, *Global Biogeochem. Cy.*, 28, 553–570, <https://doi.org/10.1002/2014GB004814>, 2014.
- Zunino, P., Lherminier, P., Mercier, H., Daniault, N., García-Ibáñez, M. I., and Pérez, F. F.: The GEOVIDE cruise in May–June 2014 revealed an intense MOC over a cold and fresh subpolar North Atlantic, *Biogeosciences*, 14, 5323–5342, <https://doi.org/10.5194/bg-14-5323-2017>, 2017.